LAWRENCE
LIVERMORE
NATIONAL
LABORATORY

LLNL-JRNL-669460

Carbyne Fiber Synthesis Within Evaporating Metallic Liquid Carbon

C. Cannella, N. Goldman

April 8, 2015

Journal of Physical Chemistry C

Disclaimer

This document was prepared as an account of work sponsored by an agency of the United States government. Neither the United States government nor Lawrence Livermore National Security, LLC, nor any of their employees makes any warranty, expressed or implied, or assumes any legal liability or responsibility for the accuracy, completeness, or usefulness of any information, apparatus, product, or process disclosed, or represents that its use would not infringe privately owned rights. Reference herein to any specific commercial product, process, or service by trade name, trademark, manufacturer, or otherwise does not necessarily constitute or imply its endorsement, recommendation, or favoring by the United States government or Lawrence Livermore National Security, LLC. The views and opinions of authors expressed herein do not necessarily state or reflect those of the United States government or Lawrence Livermore National Security, LLC, and shall not be used for advertising or product endorsement purposes.

A density functional tight binding model for carbon with dispersion: Simulations of carbyne fiber synthesis within expansions of liquid metallic carbon

Christopher B. Cannella and Nir Goldman*

Physical and Life Sciences Directorate, Lawrence Livermore National Laboratory

E-mail: ngoldman@llnl.gov

*To whom correspondence should be addressed

Abstract

We discuss the formation of carbyne fiber bundles over nanosecond time scales in laser pulse melting studies of graphite using a new dispersion correction for a density functional tight binding model for carbon under extreme conditions. Our dispersion energy model is determined by optimizing a modified Lennard-Jones style potential to an experimentally determined equation of state for graphite valid up to high pressure. This yields excellent accurate results for the graphite bulk modulus and crystalline lattice parameters under ambient conditions. We then simulate laser induced melting by heating graphite to close to the graphite/diamond/liquid triple point until it is fully melted, and then expanding along its adiabatic and cooling to low temperature. We observe the transition from a predominantly sp^2 bonded, cumulene like system to one that is almost entirely sp-bonded as the material cools and equilibrates, forming carbyne strands bound together via dispersion interactions. The high computational efficiency of our approach allows for direct comparison with experiments that span a wide range of thermodynamic conditions, and can help determine parameters for synthesis of carbon-based materials with potentially exotic properties.

1 Introduction

Though the phase diagram of carbon has been studied somewhat extensively under very extreme conditions (e.g., 10,000's of degrees Kelvin and 1000's of GPa[1,2]), its properties under dynamic conditions close to the graphite/diamond/liquid triple point (∼12GPa and 5000 K[3]) remains an open question despite several decades of research. The mass of available carbon in Neptune and Uranus could comprise approximately 17% of each total planetary mass, and the liquid phase may exist deep within these planets interiors, possibly contributing to their high magnetic moments.[4] Experimental difficulties arise in part due to the elevated temperature which can necessitate laser pulsed heating of a graphite or diamond like carbon film, followed by measurement of the rapidly expanding and boiling liquid phase.[5–7] These studies have reported a significant range of results for the average chemical bonding of the material (e.g., sp vs. sp^2 hybridization) under both hot and cooled conditions. In particular, there is a wide variety of possible expansion products that have been reported, including nanoclusters of diamond and graphite,[6] novel super dense phases,[8] and carbyne.[7]

Carbyne (e.g., polyyne, linear chains of sp-bonded carbon), is of particular interest due to its computed physical and electronic properties. It has been found in the Murchison and Allende carbonaceous chondrites,[9] and could be a constituent of interstellar dust.[10] The material is thought to be switched into a magnetic semiconductor state by mechanical twisting, and has has been proposed as a nanoelectronic/spintronic material,[11] as well as having possible use for hydrogen storage.[12] The carbyne chains themselves have been computed to be forty times stiffer than diamond with reaction barriers for cross-linking close to 14 kcal/mol,[13] possibly preventing its exothermic decomposition. Femtosecond laser pulsing experiments have observed evidence for their synthesis under ultra-high vacuum and state that the sp-bonded chains are extremely insensitive to exposure to air,[7] similar to reports on carbyne chemical synthesis in the laboratory.[14] However, only recently have there been some claims of a more reliable means of its production,[15] though these studies generally have been limited to relatively short chain lengths. These issues could be clarified to some degree

by theoretical studies of the mechanism for carbyne synthesis as well as determination of its physical and chemical properties.

Quantum simulation methods such as Kohn-Sham Density Functional Theory (DFT) hold promise as an independent route to determining the physical propeties and chemical reactivity of reactive materials during synthesis (e.g., Ref.[2]). DFT remains one of the most popular and widely used modeling methods in condensed matter physics, computational chemistry, and materials science for prediction of material properties and chemical reactivity. It has been shown to accurately reproduce the phase boundaries and thermal decomposition of many materials.[16–18] However, DFT is extremely computationally intensive, which limits its use to system nanometer system sizes picosecond time scales. In contrast, studies such as the laser melt experiments discussed here span up to micron length scales and nanosecond time scales. Molecular dynamics (MD) simulations with DFT are consequently intractable for many dynamic studies, where chemical reactivity can evolve over the entire course of the experiment. In addition, popular density functionals tend to strongly underestimate van der Waals or dispersion interactions, which can result in poor predictions for molecular crystals, π-π stacking interactions, and other chemical environments.[19] This is particularly true for carbon, where the poor representation of dispersion forces in DFT yields an extremely low bulk modulus (resistance to isotropic compression) for graphite.[20] Fully *ab initio* treatments of dispersion interactions in DFT exist,[21] though these are largely far too expensive to be of practical use, and dispersion is generally included with an *a posteriori* semi-empirical potential specific for a given exchange-correlation functional.[22,23]

Semi-empirical quantum theories such as density functional tight binding (DFTB) yield a higher degree of computationally efficiency while retaining most of the accuracy of methods such as Kohn-Sham DFT.[24,25] DFTB utilizes a minimal local atomic basis set (e.g., s and p-orbitals only on carbon) and computes electronic states from a two-center (two nuclear site) Hamiltonian and strictly pair-wise interaction potentials. These simplifications allow for all matrix elements to be pre-computed on a radial grid for rapid evaluation. DFTB

can subsequently yield several orders of magnitude increase in computational efficiency over most DFT implementations, which project the electronic density onto a fine grid, and then use Fourier transforms to compute the Hartree potential and other terms (e.g., Ref.[26]). However, the simplified Hamiltonian in DFTB can result in a complete exclusion of dispersion interactions for the total system energy.[19] Some success in solving these problems have been found with empirical dispersions corrections,[19,27] though to the best of our knowledge, these have not been developed for phase transitions in carbon specifically until now.

In this work, we improve upon a previously determined DFTB for carbon under extreme conditions[28] by determining an empirical dispersion correction through comparison to an experimentally determined equation of state for graphite up to high pressure. Our new model yields significantly improved results for the graphite ambient crystalline parameters and density, as well as its bulk modulus. We then simulate laser pulse melting of graphite to close to nanosecond timescales and detail the formation of carbyne fibers on experimentally observable time scales. Finally, we discuss the ensuing changes in bonding environments as well as the likely atomic orbital hybridization that occurs over the manifold of thermodynamic states visited during our simulations, as carbon transitions from a liquid to a one dimensional solid.

2 Results and Discussion

In order to determine the dispersion energy E_{disp} for our DFTB carbon model, we adopt a functional form similar to that of the universal force field (UFF):[29]

$$E_{disp} = \begin{cases} d_0 \left[-2 \left(\frac{r_{disp}}{r_{ij}} \right)^6 + \left(\frac{r_{disp}}{r_{ij}} \right)^{12} \right], & r_{ij} > r_{min} \\ b_0 - \sum_{n=2}^{10} b_n r_{ij}^n, & r_{ij} < r_{min} \end{cases} \tag{1}$$

Here, a Lennard-Jones style interaction is used to describe the dispersion forces at r_{ij} distances greater than the position of the potential minimum r_{min}. The tenth-order polynomial

is used to correct the pressures from our DFTB model for distances greater than r_{min}. The values of d_0, r_{disp}, and the b_n coefficients are determined through optimization. In this case, the coefficients b_5 and b_{10} were constrained to restrict the value of the polynomial and its first derivative to be zero at r_{min} in order to maintain continuity between the two equations.

Determination of E_{disp} was performed by first computing pressures from our uncorrected DFTB model for graphite at densities determined from an experimentally determined equation of state for pressures up to 14 GPa.[30] Calculation were performed with configurations of 64 atoms and up to a 10x10x10 Monkhorst-Pack mesh,[31] though pressures were found to be converged to within 1% with a 3x3x3 mesh, only. Hence, we used a 4x4x4 mesh for our optimization calculations. Simulated annealing[32] was then used to determine parameters that yield pressures that make up the difference. We further refined the dispersion energy parameters by performing geometry optimizations with the DFTB+ code[33] and our E_{disp} model at each pressure, and scaling the d_0 and b_0 parameters in order to better match the experimental results (parameters listed in Table 1). Final results (Figure 1) indicate that our DFTB model with dispersion accurately accounts for the interactions between graphitic planes during compression, whereas the uncorrected model is significantly too soft and yields a material that is too compressible.

Our new dispersion model yields strongly improved agreement with experimental results for graphite under ambient conditions (Table 2). We compute an ambient density ρ_0 that deviates 6.7% from the experimental value, compared to 23.3% for DFTB without a dispersion correction. Similarly, our model yields a c lattice constant (the lattice direction along the graphitic planes) that deviates only 4.5% from the experimental value, compared to 36.3% for DFTB without dispersion corrections. Finally, our model predicts a bulk modulus B_0 (e.g., the resistance of a material to isotropic compression) for graphite that agrees to within 3 GPa of experiment, compared to uncorrected DFTB with yields a value close to zero due to the gross underestimation of the dispersion forces.

We have applied our DFTB model with dispersion to simulations of laser melting of

graphite. All MD simulations were run with a hybrid code simulation code, with DFTB+ used to compute the atomic forces and cell stress tensor, and the LAMMPS molecular dynamics software suite[34] used to drive the dynamics. Previous results for carbon under extremely high pressures and temperatures have shown that self-consistent charge (SCC) calculations and non-SCC calculations yield virtually identical system energies, radial distribution functions, and pressures for a given temperature and density.[35,36] Here, we report on results from non-SCC simulations, only. For our simulations, we start with a configuration of 256 carbon atoms in a graphite lattice with supercell dimensions of a =13.1061 Å, b =16.6673 Å, and c =9.6056 Å. These dimensions correspond to the zero pressure density computed from our model (2.43 g/mL), and yield cell lattice vectors large enough to permit Γ-point sampling of the Brillouin zone, only. In order to produce liquid configurations we first heated our simulation cell from 300 K to 10,000 K over there course of 50 ps using a time step of 0.25 fs. We then equilibrated our simulation at 10,000 K for 30 ps using the same time step, after which we ramped the temperature down to 5000 K (the approximate temperature of experiments[5]) over the course of 30 ps and then equilibrated for an additional 30 ps.

We have validated our DFTB model with dispersion by computing a 5 ps DFT-MD trajectory at the same temperature and density using the VASP code.[37–39] DFT calculations were performed projector-augmented wave (PAW) pseudopotential[40,41] and the Perdew-Burke-Ernzerhof generalized gradient approximation functional (PBE)[42] with a planewave cutoff of 900 eV. Dispersion forces were not included in these calculations, though they are relatively small at extreme conditions. The radial distribution function (RDF) from our DFTB model compares well to results from DFT, as well as those from previous tight binding simulations at the same density but at 7000 K[43] (Figure 2). Both sets of tight binding results predict first peaks in the RDF that have a smaller height than that from DFT, and a nearest neighbor distance that is slightly smaller. However, we compute a coordination number for the first coordination shell (number of nearest neighbors) of 2.9 for both tight binding models, which corresponds closely with the value of 3.2 from DFT. In addition, we observe that the

position and height of the second coordination shell agree between all three models.

After equilibration at high temperature, the simulation cell was expanded to low density and cooled to low temperature, corresponding to the evaporation of liquid carbon observed during experiments. Adiabatic expansion simulations were conducted using the DOLLS algorithm[44]. Here, the simulation cell volume is altered at a constant rate while ensuring that the system is constrained to visit the thermodynamic states corresponding to its adiabat, i.e., $dE_{tot} = -PdV$. We expanded our simulations over the course of 250 ps to a density of ∼0.5 g/mL, approximating gas phase densities. We then ramped the temperature down from the the final expansion temperature of ∼3500 K to 100 K over an additional 250 ps. Lower conditions allowed us to increase the simulation time step to 0.5 fs. Finally, we equilibrated our simulations at 100 K for an additional 100 ps. This corresponded to a total simulation time of almost 750 ps, i.e., several orders of magnitude longer than what is accessible by standard DFT-MD simulations.

Before the onset of expansion, we observe that the system exists in a relatively high pressure and temperature state, and consists of a number of carbon atoms in ring-like structures (Figure 3), consistent with a coordination number close to a value of three. Expanding and cooling yields a number of carbyne (e.g., sp-bonded carbon) chains, that are bound together by dispersion interactions. We have analyzed the structural changes that occur during expansion and cooling by computing the RDF for both sets of trajectories (Figure 4). We observe that upon expanding to low density, the first peak of the RDF has sharpened and shifted to approximately 1.25Å, consistent with cumulene (i.e., an infinite chain of carbon double bonds), very similar to the value of 1.28 Å computed from DFT calculations.[45] At approximately 2200 K, the symmetry of the cumulene structure is broken and the system separates into alternating single and triple bonds due to the Peierls distortion. After cooling the system to 100 K, we compute a triple bond length of 1.16 Å and a single bond length of 1.33, compared to estimated values of 1.21 Å and 1.38 Å respectively.[46] Both sets of results yield bond length alternation (BLA) values of 0.17 Å, although high-level DFT calculations

with dispersion corrected functionals generally yield values around 0.09 Å for polyyne[13,47] .

In order to quantify the types of chemical bonds that form in hot, dense carbon as it expands and cools, we have computed the average coordination for each atom as a function of temperature (Figure 5). We find that at 5000 K approximately 50% of the carbon atoms are in graphite-like configurations (three-fold coordinated), 30% are in linear configurations (two-fold coordinated) and the remaining 20% are in tetrahedral configurations (four-fold coordinated). These results compare well to previous tight binding simulations[43] and are consistent with the experimental finding of a mixture of sp, sp^2, and sp^3 forms of bonding under very similar conditions.[5] The system experiences a cross-over point at approximately 2.15 g/mL and 4800 K where the fraction of atoms in graphite-like vs. linear configurations is equal at ∼45%, and the number of atoms in tetrahedral configurations has decreased to ∼10%. By the time the system has fully expanded to its low density, high temperature state, it is almost entirely comprised of linear chains with a small number of graphite-like cross-linkings. The slight increase in graphite-like atoms at ∼2200 K corresponds to the spontaneous formation of a five-membered carbon ring which forms as two cross-linking bounds between adjacent carbon-chain strands. The ring ultimately breaks apart at around the point the Peierls distortion sets in, and chains of alternating sp^3 and sp bonds are energetically favored. These findings are consistent with experimental results, which indicate that the liquid is predominantly sp-bonded at it achieves low density states.[5] Our analysis yields a simple description of the initial liquid state as it progresses towards carbyne structures during both expansion and cooling that are amenable to further measurement by time resolved x-ray absorption experiments.

3 Conclusions

We have analyzed a mechanism for carbyne formation from laser-melted graphite using a dispersion energy corrected form of the density functional tight binding method in simulations

to close to one nanosecond. The dispersion correction for our model was determined through comparison to experimental isothermal compression results for graphite, and yields accurate results for the ambient density and lattice parameters, as well as the bulk modulus. Heating ambient graphite to 5000 K yields a liquid phase that is predominantly comprised of two-fold coordinated (graphite-like) bonding. Adiabtaic expansion yields a series of linear chains likely with double bonds, which upon cooling to low temperature form strands of alternating single and triple bonds that are bundled via dispersion interactions. Our simulations indicate a possible mechanism for carbyne fiber synthesis that confirms previous experimental observation of its formation. Our results help determine one set of thermodynamic conditions for its synthesis, and could account for its detection in the interstellar space medium. Our DFTB model will have particular impact in these types of research areas, where there is traditionally a reliance on expensive DFT calculations for interpretation of imaging and spectroscopy experiments, and prediction of properties to guide materials synthesis.

4 Acknowledgments

This work was performed under the auspices of the U.S. Department of Energy by Lawrence Livermore National Laboratory under Contract DE-AC52-07NA27344, and was funded by Laboratory Directed Research and Development grant # 12-ERD-052. Computations were performed at LLNL using the Aztec massively parallel computer.

Table 1: Parameters for our dispersion model. Polynomial parameter values are listed in atomic units.

Parameter	Value
d_{ij} (kcal/mol)	0.3927
r_{disp} (Å)	3.9320
b_0	4.2881x10^{-3}
b_2	1.2398 x10^{-4}
b_3	1.5125 x10^{-5}
b_4	-3.5625 x10^{-6}
b_5	-4.1702 x10^{-7}
b_6	8.6272 x10^{-8}
b_7	1.4095 x10^{-9}
b_8	2.5304 x10^{-10}
b_9	-6.8592 x10^{-11}
b_{10}	-3.3693 x10^{-12}

Table 2: Graphite structural parameters and physical results at zero pressure.

	Density (g/mL)	a (Å)	c (Å)	B_0 (GPa)
Experiment[30]	2.29	2.47	6.71	35.8
DFT[20]	1.71	2.47	8.84	1
DFT, with dispersion[20]	2.35	2.46	6.45	38
DFTB	1.74	2.48	9.14	0.7
DFTB, with dispersion	2.43	2.40	6.55	38.5

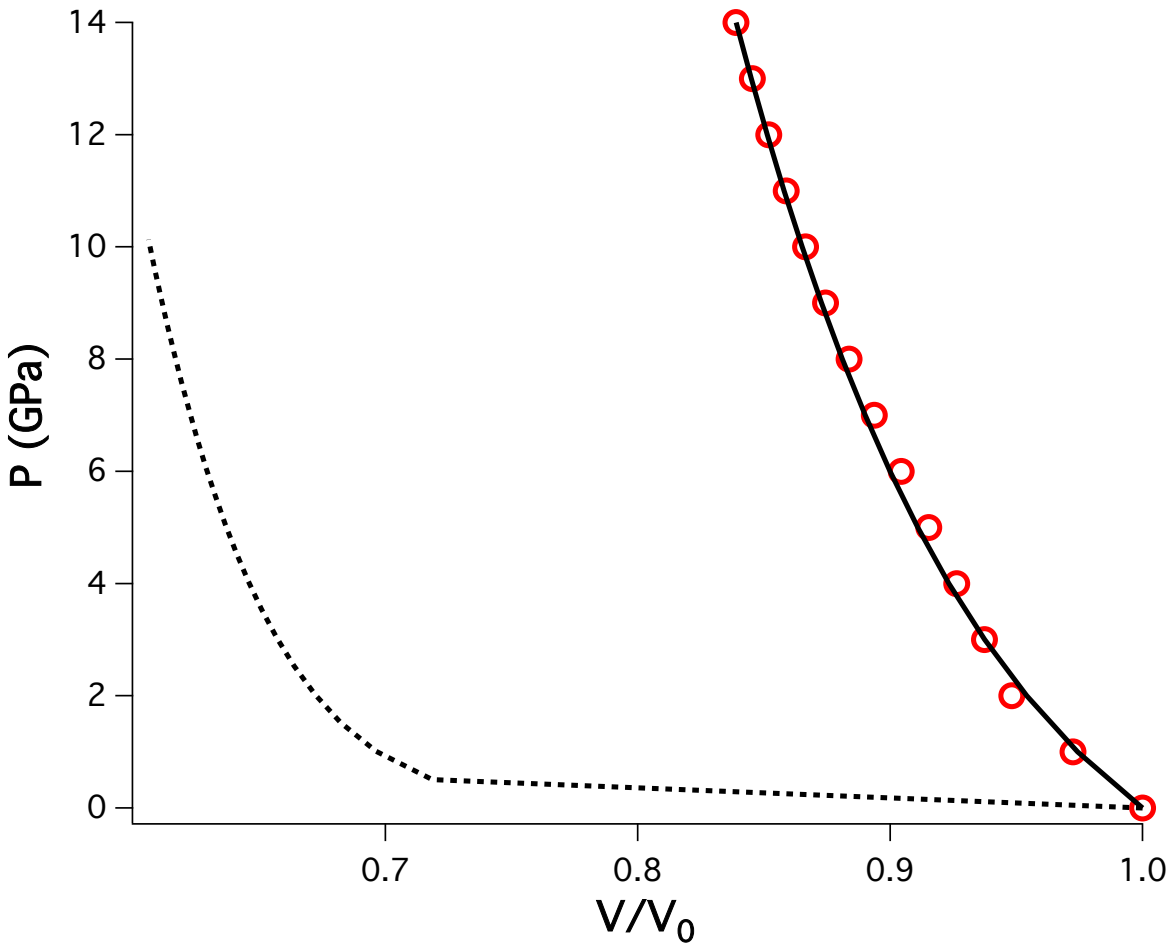

Figure 1: Graphite zero temperature compression curves. Experimental EOS results are denoted by the solid black line, DFTB without dispersion correction with the the dashed black line, and DFTB with our dispersion model with the open red circles.

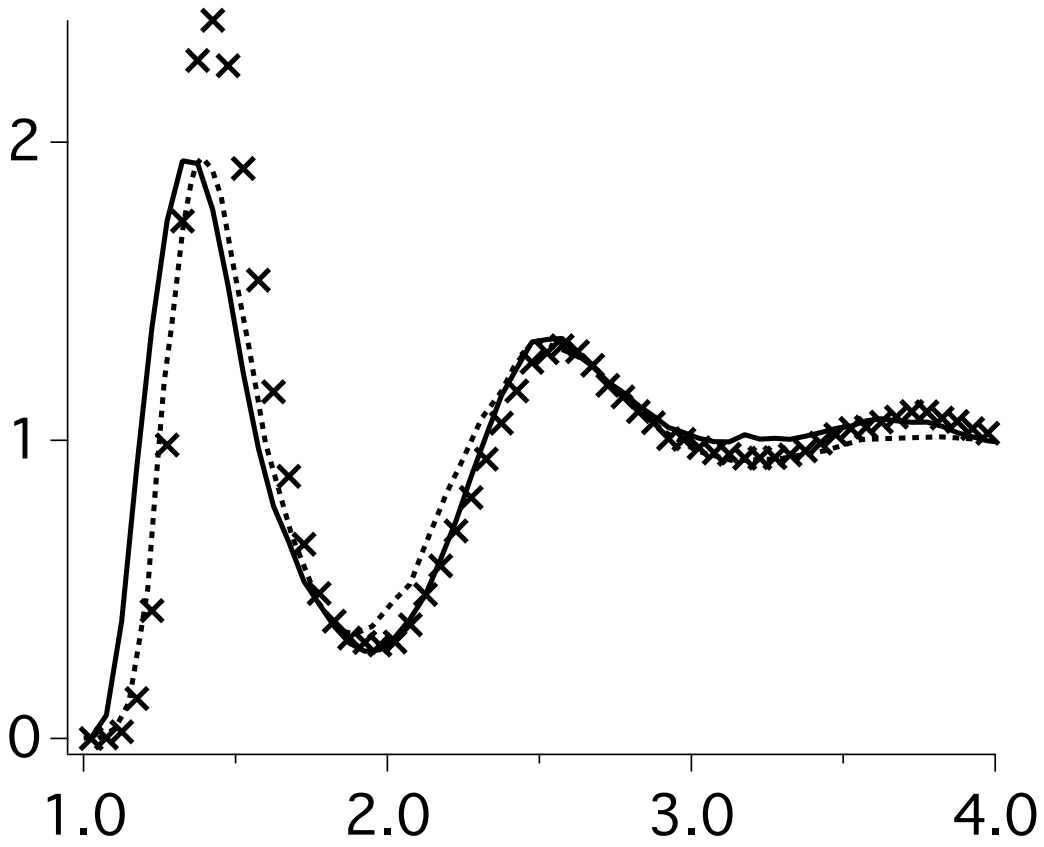

Figure 2: Radial distribution functions for liquid carbon at 2.4 g/mL. DFT calculations (X's) and DFTB calculations (solid line) were performed at 5000 K, whereas previous tight binding calculations[43] (dashed line) were performed at 7000 K.

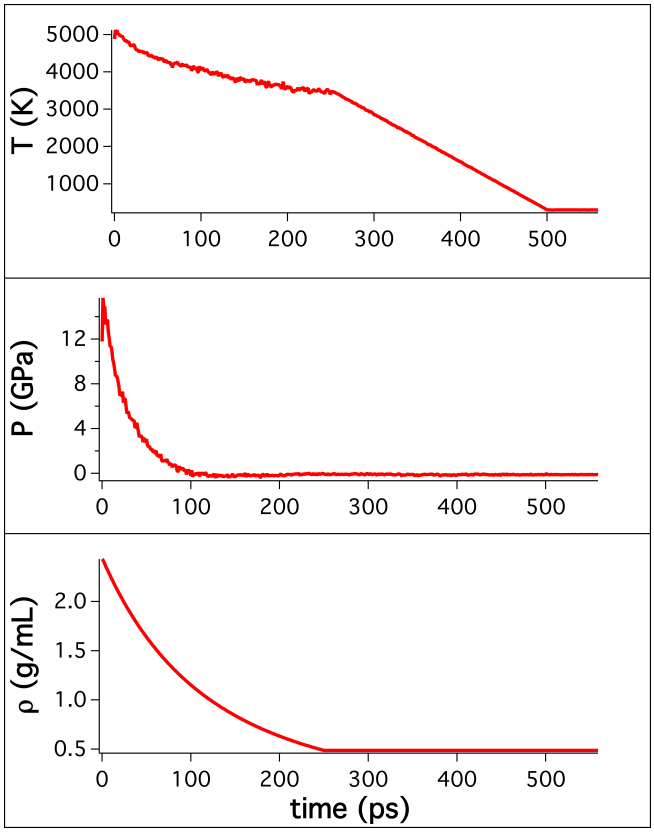

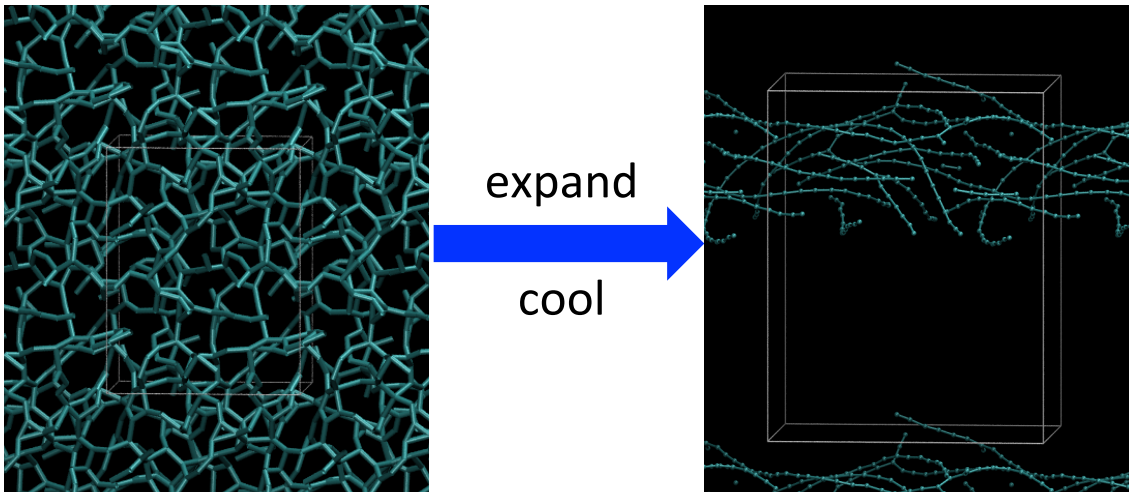

Figure 3: Equation of state time traces for our simulations as well as MD snapshots of configurations of the liquid before and after expansion and cooling to low temperature. The larger size of the simulation cell in the right panel (grey lines) corresponds to the larger system volume due to expansion.

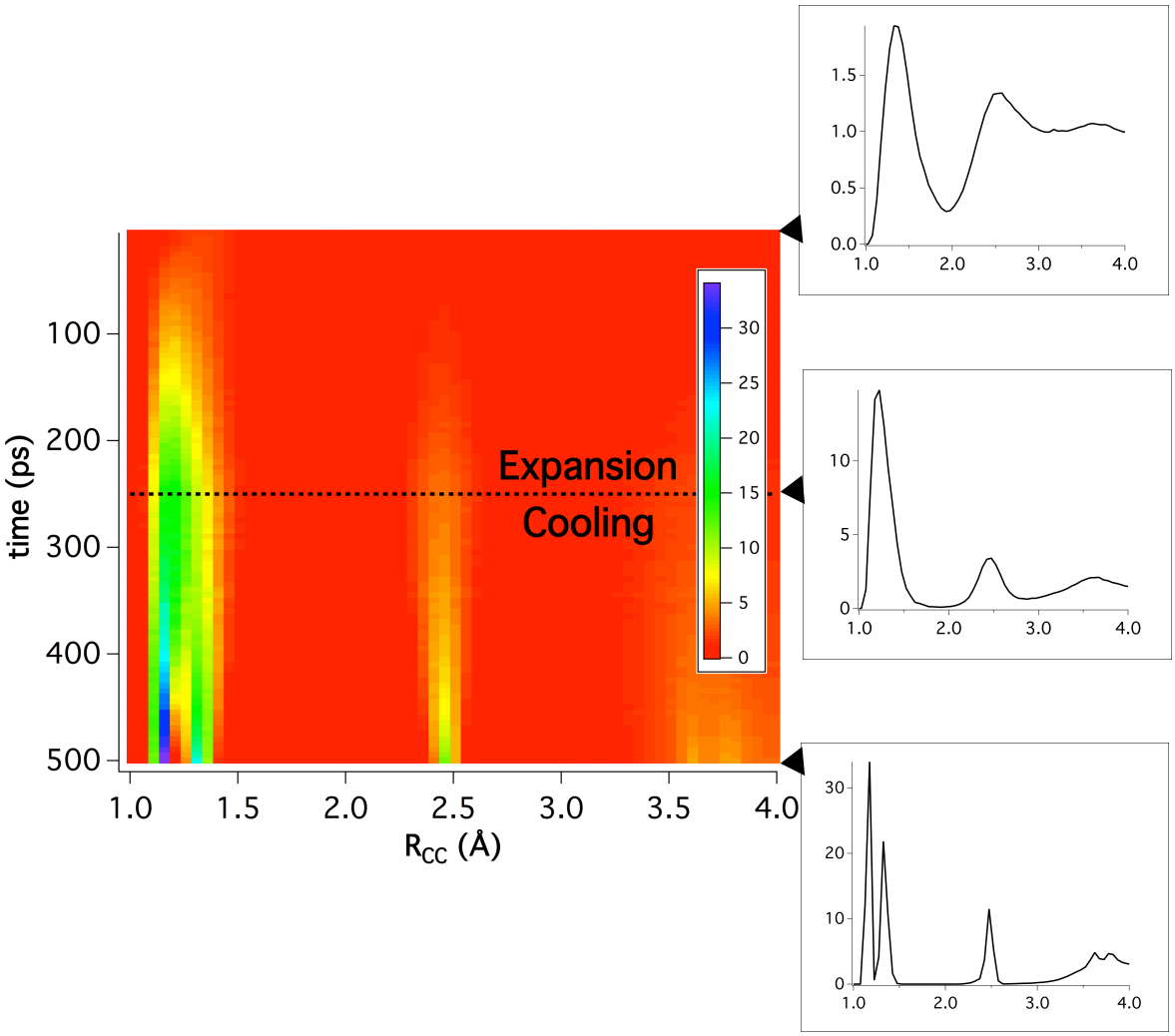

Figure 4: Radial distribution functions for carbon during the expansion and cooling steps. Alternating carbon bond lengths for carbon appear at ∼2000 K (400 ps in this plot) due to the Peierls distortion.

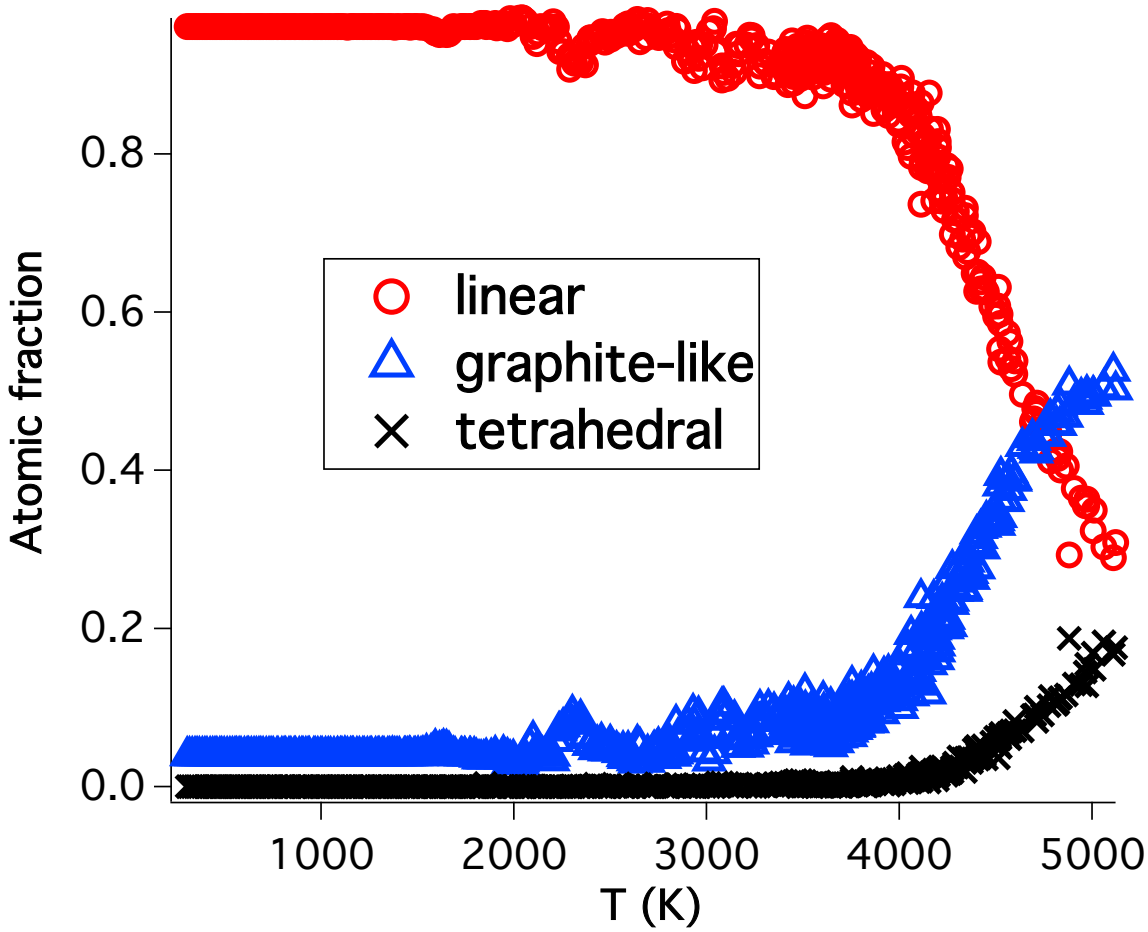

Figure 5: Fraction of carbon atoms in configurations that are either linear (two-fold coordinated), graphite-like (three-fold coordinated), or tetrahedral (four-fold coordinated) as a function of temperature. At the start of our simulations at 5000 K three-fold coordination is preferred, although two-fold coordination begins to predominates fairly early during the expansion process.

References

(1) Correa, A. A.; Bonev, S. A.; Galli, G. *Proceedings of the National Academy of Sciences of the United States* **2006**, *103*, 1204.

(2) Goldman, N.; Tamblyn, I. *The Journal of Physical Chemistry A* **2013**, *117*, 5124 – 5131.

(3) Bundy, F. P.; Bassett, W. A.; Weathers, M. S.; Hemley, R. J.; Mao, H. K.; Goncharov, A. F. *Carbon* **1996**, *34*, 141–153.

(4) Ross, M. *Nature* **1981**, *292*, 435.

(5) Johnson, S. L.; Heimann, P. A.; MacPhee, A. G.; Lindenberg, A. M.; Monteiro, O. R.; Chang, Z.; Lee, R. W.; Falcone, R. W. *Phys. Rev. Lett.* **2005**, *94*, 057407.

(6) Hu, A.; Lu, Q.-B.; Duley, W. W.; Rybachuk, M. *J. Chem. Phys.* **2007**, *126*, 154705.

(7) Hu, A.; Rybachuk, M.; Lu, Q.-B.; Duley, W. W. *Appl. Phys. Lett.* **2007**, *91*, 131906.

(8) Basharin, A. Y.; Dozhdikov, V. S.; Dubinchuk, V. T.; Kirillin, A. V.; Lysenko, I. Y.; Turchaninov, M. A. *Technical Physics Letters* **2009**, *35*, 428–431.

(9) Whittaker, A. G.; Watts, E. J.; Lewis, R. S.; Anders, E. *Science* **1980**, *209*, 1512–1514.

(10) Webster, A. *Mon. Not. Astr. Soc.* **1980**, *192*, 7P–9P.

(11) Artyukhov, V. I.; Liu, M.; Yakobson, B. I. *Nano Lett.* **2014**, *14*, 4224.

(12) Sorokin, P. B.; Lee, H.; Antipina, L. Y.; Singh, A. K.; Yakobson, B. I. *Nano Lett.* **2011**, *11*, 2660–2665.

(13) Liu, M.; Artyukhov, V. I.; Lee, H.; Xu, F.; Yakobson, B. I. *ACS Nano* **2013**, *7*, 10075–10082.

(14) Chalifoux, W. A.; Tykwinski, R. R. *Nat. Chem.* **2010**, *2*, 967–971.

(15) Kano, E.; Takeguchi, M.; Fujita, J.; Hashimoto, A. *Carbon* **2014**, *80*, 382–386.

(16) Goldman, N.; Reed, E. J.; Kuo, I.-F. W.; Fried, L. E.; Mundy, C. J.; Curioni, A. *J. Chem. Phys.* **2009**, *130*, 124517.

(17) Goldman, N.; Reed, E. J.; Fried, L. E. *J. Chem. Phys.* **2009**, *131*, 204103.

(18) Goldman, N.; Reed, E. J.; Fried, L. E.; Kuo, I.-F. W.; Maiti, A. *Nat. Chem.* **2010**, *2*, 949.

(19) Zhechkov, L.; Heine, T.; Patchkovskii, S.; Seifert, G.; Duarte, H. A. *J. Chem. Theory Comput.* **2005**, *1*, 841–847.

(20) Bučko, T.; Hafner, J.; Lebègue, S.; Ángyán, J. G. *J. Phys. Chem. A* **2010**, *114*, 11814.

(21) Marom, N.; Tkatchenko, A.; Rossi, M.; Gobre, V. V.; Hod, O.; Scheffler, M.; Kronik, L. *J. Chem. Theory Comp.* **2011**, *7*, 3944–3951.

(22) Grimme, S. *J. Comp. Chem.* **2006**, *27*, 1787–1799.

(23) Grimme, S.; Antony, J.; Ehrlich, S.; Krieg, H. *J. Chem. Phys.* **2010**, *132*, 154104.

(24) Elstner, M.; Porezag, D.; Jungnickel, G.; Elsner, J.; Haugk, M.; Frauenheim, T.; Suhai, S.; Seifert, G. *Phys. Rev. B* **1998**, *58*, 7260.

(25) Koskinen, P.; Mäkinen, V. *Comp. Mater. Sci.* **2009**, *47*, 237.

(26) Soler, J. M.; Artacho, E.; Gale, J. D.; García, A.; Junquera, J.; Ordejón, P.; Sánchez-Portal, D. *Journal of Physics: Condensed Matter* **2002**, *14*, 2745.

(27) Elstner, M.; Hobza, P.; Frauenheim, T.; Suhai, S.; Kaxiras, E. *J. Chem. Phys.* **2001**, *114*, 5149–5155.

(28) Goldman, N.; Browning, N. D. *J. Phys. Chem. C* **2011**, *115*, 11611.

(29) Rappé, A. K.; Casewitt, C. J.; Colwell, K. S.; III, W. A. G.; Skiff, W. M. *J. Am. Chem. Soc.* **1992**, *114*, 10024–10039.

(30) Hanfland, M.; Beister, H.; Syassen, K. *Phys. Rev. B* **1989**, *39*, 12598.

(31) Monkhorst, H. J.; Pack, J. D. *Phys. Rev. B* **1976**, *13*, 5188.

(32) Kirkpatrick, S.; Gelatt, C. D.; Vecchi, M. P. *Science* **1983**, *220*, 671–680.

(33) Aradi, B.; Hourahine, B.; Frauenheim, T. *J. Phys. Chem. A* **2007**, *111*, 5678, http://www.dftb-plus.info.

(34) Plimpton, S. *J. Comp. Phys.* **1995**, *117*, 1, http://lammps.sandia.gov.

(35) Goldman, N.; Fried, L. E. *J. Phys. Chem. C* **2012**, *116*, 2198.

(36) Goldman, N.; Srinivasan, S. G.; Hamel, S.; Fried, L. E.; Gaus, M.; Elstner, M. *J. Phys. Chem. C* **2013**, *117*, 7885 – 7894.

(37) Kresse, G.; Hafner, J. *Phys. Rev. B* **1993**, *47*, R558.

(38) Kresse, G.; Hafner, J. *Phys. Rev. B* **1994**, *49*, 14251.

(39) Kresse, G.; Furthmüller, J. *Phys. Rev. B* **1996**, *54*, 11169.

(40) Blöchl, P. E. *Phys. Rev. B* **1994**, *50*, 17953.

(41) Kresse, G.; Joubert, D. *Phys. Rev. B* **1999**, *59*, 1758.

(42) Perdew, J. P.; Burke, K.; Ernzerhof, M. *Phys. Rev. Lett.* **1997**, *78*, 1396.

(43) Morris, J. R.; Wang, C. Z.; Ho, K. M. *Phys. Rev. B* **1995**, *52*, 4128.

(44) Hoover, W. G.; Evans, D. J.; Hickman, R. B.; Ladd, A. J. C.; Ashurst, W. T.; Moran, B. *Phys. Rev. A* **1980**, *22*, 1690.

(45) Nori-Shargh, D.; Deyhimi, F.; Boggs, J. E.; Jameh-Bozorghi, S.; Shakibazadeh, R. *J. Phys. Org. Chem.* **2007**, *20*, 355.

(46) Heimann, R. B.; Kleiman, J.; Salansky, N. M. *Carbon* **1984**, *33*, 147–155.

(47) Yang, S.; Kertesz, M. *J. Phys. Chem. A* **2006**, *110*, 9771–9774.